Notes

Microstructural Analysis of Insoluble Polyolefins by Melt-State ^{13}C NMR at Very High Temperatures

Wei Hu,† Hideaki Hagihara,‡ and Toshikazu Miyoshi*,†

Research Institute of Nanotechnology and Research Institute for Innovation in Sustainable Chemistry, National Institute for Advanced Industrial Science and Technology (AIST), Central 5-1, Higashi 1-1-1, Tsukuba, Ibaraki 305-8565, Japan

Received February 13, 2007
Revised Manuscript Received March 15, 2007

Introduction

For polyolefins, their macroscopic properties, namely, crystallinity, crystallization temperature, lamellar thickness, and mechanical properties, are closely related to their microstructural parameters such as molecular weight, molecular weight distribution, stereoregularity, regiodefect concentration, branch length, and concentration.[1−5] Therefore, the control of such microstructural parameters is industrially and scientifically important for producing various types of polyolefins with different macroscopic properties.[1,3,4] The analysis of the microstructural parameters is also an important topic for newly synthesized polymers, and ^{13}C solution-state NMR analysis has been successfully applied to characterizing locally heterogeneous structures such as end groups, regiodefects, stereodefects,[6−11] and branch structures.[12,13] On the other hand, solution-state ^{13}C NMR analysis always suffers from the sensitivity of small signals corresponding to minor defect structures. Furthermore, by this technique, it is impossible to apply insoluble polymers such as cross-linked polyolefins and C3 branch poly(α-olefins) such as isotactic poly(3-methyl-1-butene) (iP3M1B)[14−17] and isotactic poly(3-methyl-1-penentene) (iP3M1P).[18] For such polymers, microstructural analysis cannot be realized by solution-state NMR. In these cases, fractionation by solvent extraction has been utilized as a simple and practical means of performing a rough microstructural analysis. Also, solution-state NMR was applied to the analysis of the soluble fractions and the decomposition of insoluble parts by heat treatment,[18] or of model compounds of oligomers,[15,16] or a sample with a low tacticity.[17]

To overcome sensitivity and solubility problems, melt-state NMR has also been developed for the microstructural analysis of polymers.[19−22] In the melt state, rapid dynamics in the molten state considerably averages out ^{13}C line widths broadened because of anisotropic interactions such as heteronuclear $^{1}H-^{13}C$ dipolar interactions and chemical shift anisotropy and because of conformations and disorders of chain packing. Furthermore, the combined use of typical solid-state NMR techniques, magic-angle sample spinning (MAS), and ^{1}H dipolar decoupling (DD) in the detection period further decreases the line widths. Consequently, high-resolution NMR is feasible with the solid-state NMR apparatus at high temperatures above T_m. Melt-state NMR analysis requires no solvent, and therefore, a high polymer density (a high filling factor) within the NMR coil induces a large enhancement in signal intensities. Recently, Pollard et al. have optimized experimental times using a high filling factor and a transient nuclear Overhauser enhancement (NOE) effect and concluded that the sensitivity enhancement for melt-state ^{13}C NMR is 30 times higher than that for solution-state NMR.[21] Very recently, Klimke et al. have further investigated spectral resolution and sensitivity of melt-state NMR using different NMR rotor sizes (4 and 7 mm) and those by various ^{1}H DD methods at various magnetic fields from 300 to 700 MHz.[22] They concluded that the application of a high magnetic field of 500 MHz and a 7 mm probe head provides the best sensitivity and that π decoupling effectively increases spectral resolution and allows a full observation of free induction decay (FID). Consequently, they successfully evaluated branch content with a concentration of 0.01% and copolymer contents by melt-state NMR analysis.[22]

In this work, we further aim to apply melt-state ^{13}C NMR analysis to the evaluation of stereodefects, regiodefects, and end-group structures of insoluble polyolefins at very high temperatures greater than 300 °C. Regiodefect signals show a large dispersion of the chemical shift, the values of which are different from those of regular signals, whereas stereodefect signals appear with a small shift of ∼2 ppm from the regular signals. The latter analysis, therefore, requires a high spectral resolution. First, we investigate the limitation of spectral resolution by melt-state NMR under a standard NMR magnetic field for a solid (^{1}H resonance frequency, 300 MHz) and compare the resolution with that of solution-state NMR. For this purpose, we utilize iPP, the microstructure of which has been characterized well by solution-state NMR analysis,[11−16] as a test sample. Second, we demonstrate the ^{13}C high-resolution NMR spectra of iP3M1B, which is insoluble, by melt-state NMR at very high temperatures greater than 300 °C. Consequently, the regiodefect and end-group signals as well as the main signals of iP3M1B are detected by melt-state NMR. A large sensitivity enhancement of melt-state NMR allows us to investigate relaxation time parameters and transient NOE effects on regular signals as well as on various types of defect and end-group signals. Consequently, the stereodefect and regiodefect concentrations and average molecular weight, $\bar{M}_n$, of insoluble polymers will be obtained in this work.

Experiments

The melt-state ^{13}C MAS NMR measurements at very high temperatures were conducted using a Bruker Avance 300 spectrometer, equipped with 4 and 7 mm double-resonance high-temperature NMR probes. N_2 gas was used as MAS bearing and driving gas sources in order to protect samples from oxidation and the NMR probe head. Temperature was elevated at a heating rate of 10 °C/min. During the increase in temperature, the frequency of

* Corresponding author. E-mail: t-miyoshi@aist.go.jp.
† Research Institute of Nanotechnology.
‡ Research Institute for Innovation in Sustainable Chemistry.

10.1021/ma070377q CCC: $37.00
Published on Web 04/05/2007

Table 1. Characteristics of Polymers Investigated in This Work

sample no.		$\bar{M}_n$ (g/mol)	T_m (°C)[b]
1	isotactic polypropylene (iPP)	50000	165
2	isotactic poly(3-methyl-1-butene) (iP3M1B)	2400 ± 300[a]	265
3	iP3M1B	8100 ± 1200[a]	299

[a] $\bar{M}_n$ obtained in this study by melt-state NMR. [b] Peak temperature from DSC curves recorded at heating rate of 10 °C/min.

MAS was roughly 2000 Hz in the manual mode. After reaching the target temperature above T_m of the sample, we adjusted MAS frequency to 3500 ± 5 Hz and changed to the automatic mode. The ^{1}H and ^{13}C carrier frequencies were 300.1 and 75.6 MHz, respectively. We applied the ^{13}C direct polarization (DP) method with 90° pulse lengths of 4.5−6.0 μs under high-power ^{1}H continuous-wave (CW) decoupling with field strengths of 15−50 kHz in the detecting period. This field-strength condition was carefully investigated in order to enhance spectral resolution and sensitivity. The total acquisition (ACQ) times were 150−250 ms, and the recycle delay (RD) times were 0.1−4 s. We carefully changed ACQ and RD under different decoupling conditions. In particular, weak field strengths of 15 and 25 kHz were applied to determine the RD dependence of the signal intensities for the 7 and 4 mm probes, respectively. Adjusting magnetic field homogeneity is the most important factor for obtaining high-resolution melt-state NMR spectra. We carefully adjusted magnetic field homogeneity by probing the ^{1}H line width for the CH_3 signal for the polymers used in this study. We always set the ^{1}H full line width at half-height (fwhh) to ~20 Hz at the desired temperatures. The actual temperature of the sample surroundings in NMR probes was calibrated on the basis of the temperature dependence of the ^{207}Pb chemical shift of $Pb(NO_3)_2$.[23] The ^{13}C chemical shift was referred to the CH signal of adamantane at 29.5 ppm as an external reference. ^{1}H and ^{13}C spin−lattice relaxation times in the laboratory frame, T_{1H} and T_{1C}, respectively, were obtained by the inversion recovery method.

For the 7 mm probe, pellet samples were cut into small pieces, and the samples of ~120 mg were packed into the central part of the NMR rotors. Both open spaces at the top and bottom were carefully blocked with Teflon tape with a thickness of ~2 mm. Thus, a melt-state NMR analysis of *i*PP performed at 200 °C, which is higher than equilibrium T_m. The experiment at very high temperatures greater than 250 °C was not realized using the 7 mm high-temperature MAS probe under our desired conditions (MAS 3.5 kHz, maximal supply of N_2 gas at a pressure of 0.6 MPa). The 4 mm high-temperature MAS NMR probe was used at higher temperatures above 250 °C. In this experiment, an ~40 mg sample that was melt-crystallized was inserted into the central part of NMR rotors. Teflon tape with a thickness of ~1 mm was also used to block the spaces at the top and bottom of the rotors. From our experience, packing of neat powder sometimes induces a sample crash during the heating process at around T_m due to a large volume change following melting. A high-temperature MAS experiment using the 4 mm probe was performed at 285 and 315 °C.

Solution-state ^{13}C NMR was performed on a JEOL GSX-270 equipped with a 5 mm liquid-state NMR probe at 145 °C. The ^{1}H and ^{13}C resonance frequencies were 270.1 and 67.8 MHz, respectively. The ^{13}C 90° pulse length, RD time, and ACQ time were 10 μs, 2 s, and 1.7 s, respectively. A 40 mg sample was dissolved in 5 mL of tetrachloroethane-d_2 (typical concentration in solution-state NMR analysis, 8 wt %).

Here, we investigate the microstructures of two types of sample, namely, iPP (sample 1) and two iP3M1B samples with different T_m's (samples 2 and 3) listed in Table 1. Sample 1 was purchased from Polysci. and had T_m = 165 °C. Samples 2 and 3 were synthesized in our laboratory, using C_2 symmetric homogeneous methallocene, namely, *rac*-dimethylsilylenebis(2-methyl-4-phenyl-1-indenyl)zirconium(IV) dichloride and *rac*-dimethylsilylenebis-(2-methyl-indenyl)zirconium(IV) dichloride, respectively, with a cocatalyst of MAO. Sample 2 was polymerized for 60 h at −20 °C, and its productivity was low at 6%. A reasonable amount of sample 3 was obtained by polymerization for 3 h at 20 °C. The former and latter have apparently different T_m's of 265 and 299 °C, respectively. More details of synthesis conditions are given in ref 24.

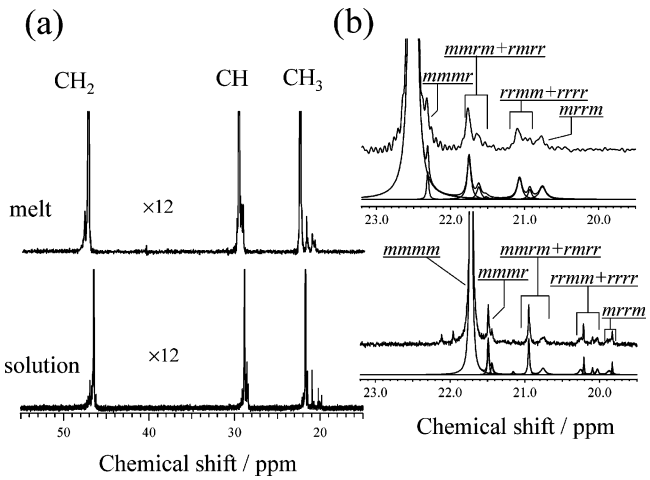

Figure 1. (a) ^{13}C melt-state and solution-state NMR spectra of iPP (sample 1) obtained at 200 and 145 °C, respectively, and (b) expansion of CH_3 region and signal assignments. The experimental conditions for the melt-state NMR are as follows: NMR probe, 7 mm high-temperature probe; CW decoupling, 25 kHz; ACQ time, 250 ms; duty factor, 11%. Lorentzian peak analysis results are also shown. The spectra are amplified 12 times along the vertical side.

Results and Discussion

Figure 1a shows ^{13}C solution-state and melt-state NMR spectra of sample 1 obtained at a recycle delay (RD) of 2 s. There are many reports on the solution-state NMR spectra of iPP, and spectral assignments are detailed in the literature[6−11] and shown in Figure 1a. The solution-state NMR analysis gives a S/N ratio of 360, and the experimental time is 75 h. The CH, CH_2, and CH_3 carbon signals show the main peaks assigned to stereoregular signals and minor and multiple peaks corresponding to well-known stereodefect signals at the bottom of the main peaks. The melt-state NMR analysis provides a similar S/N ratio of 350 within a much shorter experimental time of 1 h using the 7 mm probe and a 120 mg sample. Even though there is a large difference between the sample volumes, the melt-state NMR analysis significantly saves experimental time by a factor of 75, as indicated by Pollard et al.[21] The melt-state NMR spectrum also shows a spectral pattern similar to that in the solution state, although the chemical shifts for all the resonances move by ~0.7 ppm to the downfield side. Many factors such as polymer structure (such as conformation and chain packing), the solvent-free effect, and temperature may contribute to the observed shift for all the signals in the melt-state NMR. The line widths for the CH_3 main signal corresponding to the *mmmm* structure at the fwhh obtained by the solution-state and melt-state NMR analyses are 1.0 and 4.5 Hz, respectively, indicating that the resolution of the melt-state NMR spectrum is about 4 times lower than that of the solution-state NMR spectrum. However, the resolution achieved in our study is much better than those achieved in the previous results of melt-state NMR analysis[19−21] and is similar to the highest resolution obtained by Klimke et al. in a high magnetic field of 500 MHz.[22] Such high spectral resolution and sensitivity are attributed to a properly adjusted magnetic field homogeneity, a long ACQ time of 250 ms, a strong CW DD field strength of 25 kHz, a RD of 2 s, and a low viscosity of polymer melt at a high temperature

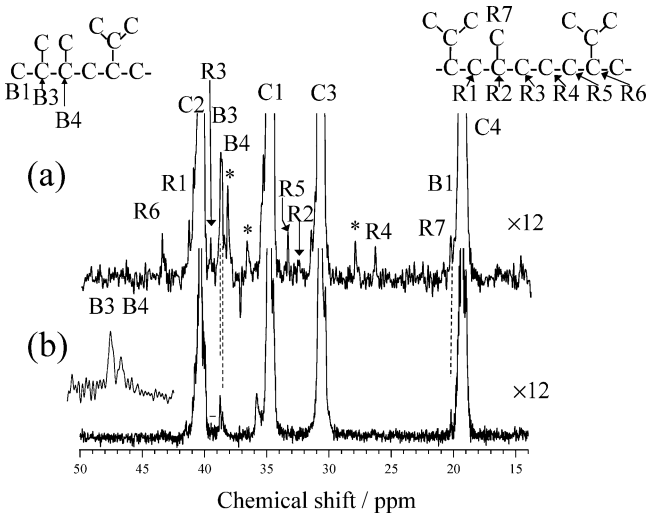

Figure 2. ^{13}C melt-state NMR spectra of iP3M1B, samples 2 (a) and 3 (b), obtained using 4 mm high-temperature NMR probe at 285 and 315 °C, respectively. The experimental conditions are as follows: CW decoupling, 50 kHz; ACQ time, 150 ms; RD time, 500 ms; duty cycle, 23%. Regiodefect and end-group structures and their assignments are inserted. * marks show unassigned signals. The spectra are amplified 12 times along the vertical side.

of 200 °C. Under these conditions, the duty cycle obtained from RD and ACQ times is 11%, which is a very severe condition for the NMR hardware. In this regard, Klimke et al. applied π decoupling, which gives a smaller duty cycle.[22]

The observed and relative peak intensities and shapes for each function signal in the melt-state NMR spectrum are similar to those in the solution-state NMR spectrum. The expanded signals for the CH_3 region and their signal assignments corresponding to stereodefects are inserted in Figure 1b. The isotacticity determinations of *mmmm* by melt-state and solution-state NMR analyses were performed by adopting Lorentzian peaks, and the former and the latter consequently yielded isotacticities of 90.6 and 90.3%, respectively. Even though the spectral resolution is much lower than that in the solution-state NMR spectrum, only a minor difference of 0.3% appears between the results of the two methods. This indicates that melt-state NMR analysis is also useful for the characterization of stereoregularity of polymers.

So far, many authors have focused on the synthesis and characterization of iP3M1B with an extremely high T_m; however, microstructural analysis has been unsuccessful except for a low-tacticity sample.[14−17,25] This is a crucial drawback for the optimization of synthesis conditions and the production of high-performance materials. Figure 2 shows the ^{13}C melt-state NMR spectra of samples 2 and 3 at very high temperatures of 285 and 315 °C, respectively. The observed ^{13}C main resonances for the main chains CH_2 (C1) and CH (C2) and side chains CH (C3) and CH_3 (C4) roughly indicate only single resonances with very small shoulders, indicating high isotacticity.[17] The detailed analysis of isotacticity will be reported elsewhere.[24] Here, we focus on other small peaks that correspond to regiodefects and end groups that appear at the chemical shift positions separated from the main resonance peaks. Previously, Borriello et al.[15] and Rishina et al.[16] observed end groups and regiodefects in iP3M1B oligomers as a model compound by solution-state NMR. In fact, Figure 2 shows the presence of end-group and regiodefect structures, those were observed in oligomers, in samples 2 and 3. The detected end-group and regiodefect structures are also shown in Figure 2. Apparently, sample 2 shows much higher intensities for the end-group and

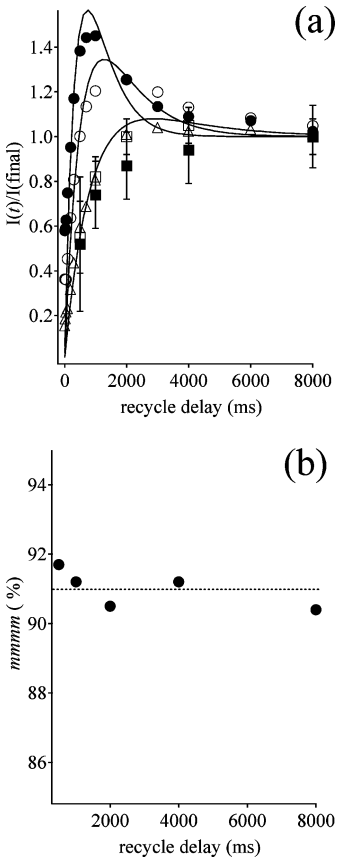

Figure 3. RD dependences of intensities of ^{13}C regular CH (○), CH_2 (●), and CH_3 (△) signals and CH_3 stereodefect, namely, ⟨*mmmr*⟩ (□) and ⟨*mmrm* + *rmrr*⟩ (■), signals with CW decoupling field of 15 kHz for ACQ time of 150 ms. The solid curves are curves best-fitted to the experimental results obtained using the equation described in the text. (b) RD dependence of the stereoregularity *mmmm* obtained by adopting Lorentzian peaks for ^{13}C CH_3 multiple signals. The dotted line is inserted at an average value of 91% as a visual guide for the readers.

regiodefect signals than sample 3. We do not show quantitative analysis of such microstructures of iP3M1B here. However, melt-state NMR results for microstructural differences in samples 2 and 3 reasonably explain the large difference between the T_m's of 265 (sample 2) and 299 °C (sample 3).

To evaluate stereoregularity, regiodefect concentration, and average molecular weight, one must wait for complete relaxation to the equilibrium state at RD time $>5T_{1C}$. So far, there have been many reports on the analysis of stereoregularity and regiodefect concentration for iPP by solution-state NMR.[6−11] Nevertheless, there are no reports on relaxation parameters for minor defect signals of iPP.[26] In fact, the reported RD time has been scattered between 2 and 12 s.[6−11] The microstructures obtained at different RD times have not been compared with each other. The large enhancement in NMR sensitivity in the melt-state NMR analysis allows us to investigate the RD dependence of the intensities of NMR signals for not only regular signals but also defect signals with minor intensities. The RD dependences of the intensities of NMR signals in the solution- and melt-state NMR are dominated by T_{1C}, T_{1H}, and a transient NOE factor due to fast molecular dynamics.[21,27,28] Figure 3a shows the RD dependences of the stereoregular signal intensities of CH_2 (●), CH (○), and CH_3 (△) carbons. The intensities of CH (○) and CH_2 (●) signals increase in the initial period and reach their maxima with enhancement factors of 1.2 and 1.4, respectively, at a RD of 1 s and finally decrease to the equilibrium state. On the other hand, the intensity of the CH_3 signal (△) gradually increases to the equilibrium state, as

Table 2. T_{1C}, T_{1H}, and a Transient NOE Factor (η) for Stereoregular Signals for iPP (Sample 1) and iP3M1B (Sample 2) Obtained at 200 and 285 °C, Respectively

	T_{1C}/ms[a]	T_{1H}/ms[a]	η[b]
sample 1			
CH	980 ± 20	790 ± 20	2.3 ± 0.3
CH2	550 ± 15	500 ± 10	2.5 ± 0.3
CH3	1950 ± 60	900 ± 15	2.1 ± 0.3
sample 2			
C2	440 ± 20	430 ± 80[c]	2.2 ± 0.5
C1	270 ± 5	405 ± 60[c]	2.0 ± 0.4
C3	460 ± 20	520 ± 10	2.3 ± 0.3
C4	2200 ± 20	700 ± 10	2.0 ± 0.3

[a] Relaxation time obtained by inversion recovery method. [b] η obtained from RD dependence of NMR signals using $I(t)/I_{eq} = 1 + (\eta/(1 - T_{1C}/T_{1H})) \exp(-t/T_{1H}) - (1 + (\eta/(1 - T_{1C}/T_{1H}))) \exp(-t/T_{1C})$. [c] Relaxation times obtained using the above equation for the overlapped ^{1}H signals.

observed in a solid-type relaxation. The RD dependences of the NMR signal intensities are represented in terms of $I(t)/I_{eq} = 1 + (\eta/(1 - T_{1C}/T_{1H})) \exp(-t/T_{1H}) - (1 + (\eta/(1 - T_{1C}/T_{1H}))) \exp(-t/T_{1C})$.[21,27,28] We measured T_{1H} and T_{1C} for all the regular signals separately, and the obtained results are listed in Table 2. The RD dependences of the signal intensities were fitted by the equation with the floating parameter, η, at fixed T_{1H} and T_{1C}. The best-fitted results are shown as solid curves in Figure 3a, and the obtained values are listed in Table 2. The η values are similar for individual carbons of iPP, and a similar η was obtained for the PE melt.[29] The T_{1H}/T_{1C} ratios for the CH and CH_2 carbons are 0.80 and 0.90, respectively, whereas that for the CH_3 carbon is only 0.46. This small value significantly contributes to the apparent solid-type curve of the RD dependence of CH_3 signal intensities.

The RD dependences for the intensities of CH_3 stereodefect, namely, ⟨*mmmr*⟩ (□) and ⟨*mmrm* + *rmrr*⟩ (■), signals are also inserted in Figure 3a. The error bars represent the inverse of the S/N ratio. The different stereodefect signals exhibit curves similar to that of the stereoregular signal (*mmmm*). This suggests that relaxation parameters and the NOE factor for defect signals are almost consistent with those for regular signals and that all RD times in our experimental ranges can be used for the evaluation of isotacticity before a full relaxation. Figure 3b shows apparent isotacticity on a pentad level as a function of RD time. As expected from similar attenuation curves for the stereoregular and defect signal intensities in Figure 3a, isotacticity is almost independent of RD, and all data are within 91.0 ± 0.8% (Figure 3a, dotted line, 91.0%). It is, therefore, possible to evaluate stereoregularity at any RD time before a full relaxation in order to determine stereodefects before complete relaxation (CH_3 ^{13}C $T_1 = 1.9$ s), if defect signals exhibit a similar RD dependence to the regular signals. However, one must take care of a short RD time that leads to a high duty factor. In fact, we used an RD time and an ACQ of 2 s and 250 ms, respectively, as experimental conditions for the full observation of FID of iPP.

The relaxation parameters and the RD dependences of the intensities of regular signals for iP3M1B as well as the regiodefect and end-group signals are investigated in the same manner as those for iPP. Figure 4a shows the RD dependences of the intensities of regular C2 (●) and C3 (□) and C4 (×) signals for sample 2. As observed in iPP, apparent enhancements in the intensities of both ^{13}C CH signals for iP3M1B are observed at a RD time of 500 ms, except for C4 carbon. The enhancement at a shorter RD time than that for iPP is attributed to the shorter T_{1C} and T_{1H} values of iP3M1B, which were separately obtained by the inversion recovery method and listed

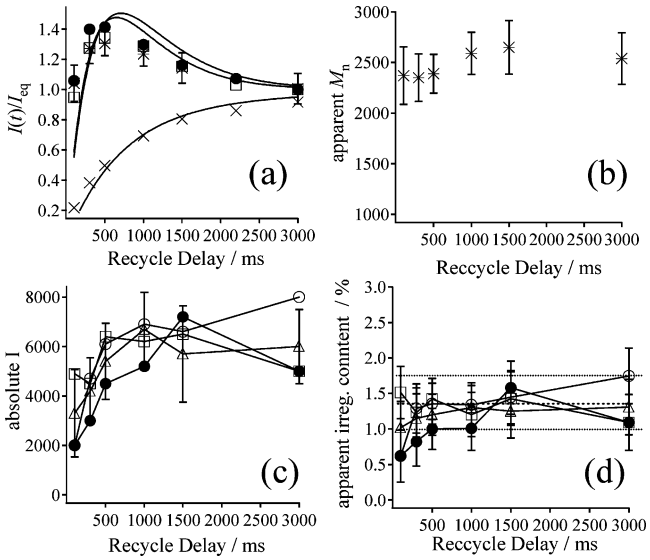

Figure 4. (a) RD dependences of intensities of ^{13}C C2 (●), C3 (□), and C4 (×) signals and end-group B3 signal (*) for sample 2 under ^{1}H CW decoupling of 25 kHz at 285 °C. The solid curves are curves best-fitted to the experimental results obtained using the equation described in the text. (b) RD dependence of $\bar{M}_n$ obtained by Lorentzian peak fitting for ^{13}C B3 and C2 signals. (c) RD dependences of intensities of regiodefect R2 (△), R3 (●), R5 (□), and R6 (○) signals for iP3M1B. (d) RD dependence of apparent regiodefect concentration calculated from peak areas of ^{13}C regiodefects and C2 signals by adopting Lorentzian peaks. The dashed and dotted lines are inserted at 1.4 and ±0.4%, respectively, as visual guides for the readers.

in Table 2. The solid curves in Figure 4a show the result best-fitted to the experimental results. The obtained η values are also shown in Table 2. In addition, the RD dependence of the intensity of the B3 signal (*)[15,16] is also shown in Figure 4a, which, surprisingly, shows a very similar tendency to both regular CH carbon signals. This result is supported by the ^{13}C T_1 for the B3 end-group signal being 460 ± 20 ms, which is similar to those of the regular C2 and C3 signals (Table 2). Consequently, the apparent $\bar{M}_n$ values obtained using B3 and C2 signal areas are almost independent of RD time, as plotted in Figure 4b. A M_n of 2400 ± 300 was obtained at a RD time of 500 ms. The regular signals for the C1 to C4 carbons in sample 3 also show similar RD tendencies for individual carbons in sample 2 (data are not shown). Therefore, using the signal intensities, the $\bar{M}_n$ of sample 3 is also evaluated to be 8100 ± 1200. In addition, the RD dependences of the intensities of the minor peaks corresponding to the regiodefect signals for sample 2 are also shown in Figure 4c. The signals also show their maximum intensities at 0.5−1.5 s, although data are scattered because of low intensity, suggesting that the relaxation and transient NOE behaviors for regiodefect signals are close to those for the C2 and C3 signals. The apparent concentration of defects determined using individual defect and C2 signals at ∼40 ppm is also shown in Figure 4d. At the shortest RD time of 100 ms, signal intensities indicate a relatively low concentration, and at longer times ≥300 ms, the results show a regiodefect concentration of 1.4% within an error of 0.4%. This suggests that the regiodefect concentration is evaluated at a relatively rapid RD time ≥300 ms. The melt-state NMR spectrum shown in Figure 2 was obtained at a RD time of 500 ms. Such a short RD time and a transient NOE effect considerably reduce the experimental time to within 3 h for each NMR spectrum of iP3M1B shown in Figure 2 and are useful for the characterization of the $\bar{M}_n$ and regiodefect concentration of iP3M1B.

In summary, we have successfully performed a melt-state ^{13}C NMR analysis of highly stereoregular polyolefins including

minor end-group and regiodefect structures at very high temperatures greater than 300 °C. The optimized resolutions under MAS and ^{1}H DD allow us to characterize stereodefect, regiodefect, and end-group structures, although the spectral resolution of melt-state NMR is still less than that of solution-state NMR. Nevertheless, a large sensitivity enhancement allows us to investigate the RD dependences of signal intensities dominated by T_{1H}, T_{1C}, and NOE behaviors. Consequently, it was possible to evaluate the components of structural defects and $\bar{M}_n$ at relatively short recycle delays of 0.5−2 s, thereby enabling the determination of $\bar{M}_n$, regiodefect concentration, and stereoregularity even for insoluble polymers. Using this technique, we will further investigate the effects of catalysts and polymerization conditions on the synthesis of C3 branch polyolefins, which have an extremely high T_m among polyolefins.[24] Melt-state NMR at a very high temperature of ∼300 °C can be applied to the microstructural analysis of many types of homopolymer as well as multicomponent systems suffering from low NMR sensitivity.

Acknowledgment. The authors thank the New Energy and Industrial Technology Development Organization (NEDO) and the Japan Society for the Promotion of Science (JSPS) for their support of this work.

References and Notes

(1) Brintzinger, H. H.; Fisher, D.; Müllhaupt, R.; Rieger, B.; Waymouth, R. M. *Angew. Chem., Int. Ed. Engl*. **1995**, *34*, 1143−1170.
(2) Marigo, A.; Marega, C.; Saini, R.; Camurati, I. *J. Appl. Polym. Sci.* **2001**, *79*, 375−384.
(3) De Rosa, C.; Auriemma, F.; Di Capua, A.; Resconi, L.; Guidotti, S.; Camurati, I.; Nifant'ev, I. E.; Laishevtsev. I. P. *J. Am. Chem. Soc.* **2004**, *126*, 17040−17049.
(4) De Rosa, C.; Auriemma, F. *J. Am. Chem. Soc.* **2006**, *128*, 11024−11025.
(5) Shroff, R.; Prasad, A.; Lee, C. *J. Polym. Sci., Polym Phys.* **1996**, *34*, 2317−2333.
(6) Schilling, F. C.; Tonelli, A. E. *Macromolecules* **1980**, *13*, 270−275.
(7) Grassi, A.; Zambelli, A.; Resconi, L.; Albizzati, E.; Mazzocchi, R. *Macromolecules* **1988**, *21*, 617−622.
(8) Busico, V.; Cipullo, R.; Chadwick, J. C.; Modder, J. F.; Sudmeijer, O. *Macromolecules* **1994**, *27*, 7538−7543.
(9) Deng, H.; Winkelbach, H.; Taeji, K.; Kaminsky, W.; Soga, K. *Macromolecules* **1996**, *29*, 6371−6376.
(10) Busico, V.; Cipullo, R.; Monaco, G.; Vacatello, M.; Segre, A. L. *Macromolecules* **1997**, *30*, 6251−6263.
(11) Busico, V.; Cipullo, R.; Monaco, G.; Vacatello, M.; Bella, J.; Serge, A. L. *Macromolecules* **1998**, *31*, 8713−8719.
(12) Liu, W.; Ray, D. G., III; Rinaldi, P. L. *Macromolecules* **1999**, *32*, 3817−3819.
(13) Shroff, R. N.; Mavridis, H. *Macromolecules* **2001**, *34*, 7362−7367.
(14) Stehling, U.; Diebold, J.; Kirsten, R.; Röll, W.; Brintzinger, H. H. Jüngling, S.; Mülhaupt, R.; Langhauser, F. *Organometallics* **1994**, *13*, 964−970.
(15) Borriello, A.; Busico, V.; Cipullo, R.; Chadwick, J. C.; Sudmeijer, O. *Macromol. Rapid Commun.* **1996**, *17*, 589−597.
(16) Rishina, L. A.; Galashina, N. M.; Nedorezova, P. M.; Klyamkina, A. N.; Aladyshev, A. M.; Tsvetkova, V. I.; Kleiner, V. I. *J. Polym. Sci., Ser. A* **2003**, *45*, 209−214.
(17) Asakura, T.; Nakayama, N. *Polym. Commun*. **1991**, *32*, 213−216.
(18) Zambelli, A.; Ammendola, P.; Sacchi, M. C.; Locatelli, P.; Zannoni, G. *Macromolecules* **1983**, *16*, 341−348.
(19) Zieglar, R. C. *Macromol. Symp*. **1994**, *86*, 213−227.
(20) Hatfield, G. R.; Kllinger, W. E.; Zeigler, R. C. *Anal. Chem.* **1995**, *67*, 3082−3085.
(21) Pollard, M.; Klimke, K.; Graf, R.; Spiess, H. W.; Wilhelm, M.; Sperber, O.; Piel, C.; Kaminsky, W. *Macromolecules* **2004**, *37*, 813−825.
(22) Klimke, K.; Parkinson, M.; Piel, C.; Kaminsky, W.; Spiess, H. W.; Wilhelm, M. *Macromol. Chem. Phys.* **2006**, *207*, 382−395.
(23) Takahashi, T.; Kawashima, H.; Sugisawa, H.; Baba, T. *Solid-State NMR* **1999**, *15*, 119−123.
(24) Hu, W.; Hagihara, H.; Miyoshi, T. *Macromolecules* **2007**, *40*, 1763−1766.
(25) Atarashi, Y. *J. Polym. Sci., Part A* **1970**, *8*, 3359−3366.
(26) Inoue, Y.; Nishioka, A.; Chûjô, R. *Macromol. Chem.* **1973**, *168*, 163−172.
(27) Okamoto, D. T.; Cooper, S. L.; Root, T. W. *Macromolecules* **1992**, *25*, 3301−3303.
(28) Alamo, R. G.; Blanco, J. A.; Carrilero, I.; Fu, R. *Polymer* **2002**, *43*, 1857−1865.
(29) Qiu, X.; Ediger, M. D. *Macromolecules* **2000**, *33*, 490−498.

MA070377Q